THE JOURNAL OF PHYSICAL CHEMISTRY C
A JOURNAL OF THE AMERICAN CHEMICAL SOCIETY

pubs.acs.org/JPCC

Article

Catalytic Reduction of Carbon Dioxide on the (001), (011), and (111) Surfaces of TiC and ZrC: A Computational Study

Fabrizio Silveri,* Matthew G. Quesne, Francesc Viñes, Francesc Illas, C. Richard A. Catlow, and Nora H. de Leeuw

Cite This: *J. Phys. Chem. C* 2022, 126, 5138−5150

Read Online

ACCESS | Metrics & More | Article Recommendations | Supporting Information

ABSTRACT: We present a computational study of the activity and selectivity of early transition-metal carbides as carbon dioxide reduction catalysts. We analyze the effects of the adsorption of CO_2 and H_2 on the (001), (011), and metal-terminated (111) surfaces of TiC and ZrC, as carbon dioxide undergoes either dissociation to CO or hydrogenation to COOH or HCOO. The relative stabilities of the three reduction intermediates and the activation energies for their formation allow the identification of favored pathways on each surface, which are examined as they lead to the release of CO, HCOOH, CH_3OH, and CH_4, thereby also characterizing the activity and selectivity of the two materials. Reaction energetics implicate HCO as the key common intermediate on all surfaces studied and rule out the release of formaldehyde. Surface hydroxylation is shown to be highly selective toward methane production as the formation of methanol is hindered on all surfaces by its barrierless conversion to CO.

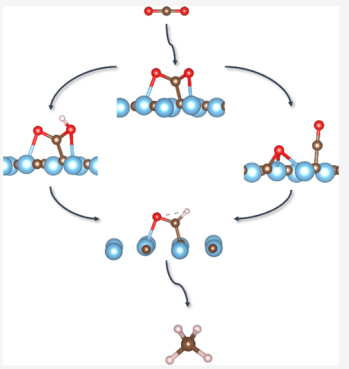

INTRODUCTION

The growing awareness and impact of climate change have led to ambitious sustainable development goals in all sectors of the industry. Carbon capture and utilization schemes are one of the many routes that have been proposed to increase the environmental sustainability of the transport and chemical industries. The aim of this strategy is to close the cycle of fossil fuel burning by using renewable energy to recycle water and carbon dioxide into fuels and chemicals, thereby mimicking the outcome of natural photosynthesis.[1,2]

The synthetic fixation of CO_2 into fuels and chemicals can be performed through two main strategies: by sequestering CO_2 into existing molecular frameworks without changing its oxidation state or by reducing the CO_2 into base chemicals that can be further processed. While the former strategy has already been implemented in several industrial processes as a means of reducing the environmental impact of an industrial process by recycling the emitted CO_2, its use is limited by the demand for chemicals that can be produced through either exothermic or mildly endothermic reactions—typically urea, carbonates, and polymers[3]—which are several orders of magnitude lower in carbon density than the global carbon emissions.[4] In contrast, direct carbon dioxide reduction with water or other readily available natural chemicals is a highly endothermic process, requiring either large amounts of energy or the use of highly reductive chemicals to obtain the desired product. Several processes have been proposed for CO_2 recycling using the oxidation of renewably generated H_2 to provide the energy required for the reaction, which often makes use of technology that is already employed by the chemical industry. Target chemicals for CO_2 reduction can be CO, HCOOH, CH_3OH, and CH_4, which can either be used as fuels or transformed into a variety of fuels and chemicals using the technology currently employed by the chemical industry.[1,5] The reduction reactions, however, often produce a mixture of these and other carbon-based products, making selectivity an issue that must be tackled as much as activity, since the separation of chemicals can be a complex and expensive process.[6] For this reason, several studies have investigated the product selectivity of CO_2 reduction over various catalysts, and theoretical effort has often focused on this aspect of the catalytic reduction to provide insight into the design of suitable catalysts.[7−9]

The computational investigation of the catalytic activity of CO_2 reduction over Mo_2S was able to correlate its remarkable selectivity toward CO (with a ratio of 154:1 to CH_3OH), with its computed oxygen binding energy.[10] In addition, adsorption studies were performed on copper catalysts with metal oxide support, predicting higher activity at the interface between the two materials as a result of the preferential binding of H_2 on the metal, while CO_2 favors adsorption on the oxide.[6] The effect of oxygen vacancies and surface morphology on carbon dioxide activation has been highlighted by similar studies on

Received: November 30, 2021
Revised: February 16, 2022
Published: March 14, 2022

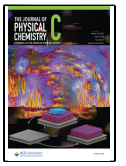

Downloaded via 80.43.159.90 on March 28, 2022 at 12:40:01 (UTC).
See https://pubs.acs.org/sharingguidelines for options on how to legitimately share published articles.

ACS Publications

© 2022 The Authors. Published by American Chemical Society

https://doi.org/10.1021/acs.jpcc.1c10180
J. Phys. Chem. C 2022, 126, 5138−5150

Cu_2O, In_2O_3, and TiO_2.[11] The reaction pathway has been investigated in several studies, identifying two recurring processes, which are selected by the site of first hydrogenation of CO_2: if this is on the carbon atom, producing an HCOO species on the catalyst surface, the first step is rate-determining and the catalyst cannot produce CO, as the product will necessarily be hydrogenated; however, if the first hydrogenation involves the oxygen, the selectivity will depend on the relative rates of CO desorption and CO hydrogenation, as the latter will be the rate-determining step for methanol formation.[12] In some cases, the mechanism was reported to change depending on the surface stoichiometry of the material, e.g., molybdenum carbides, for which combined computational and experimental studies have highlighted how selectivity toward either CO or CH_3OH is driven through a complex set of reactions by the carbon/metal ratio of the exposed surface.[13] Transition-metal carbides of groups 4−6 have been investigated both experimentally and computationally for CO_2 reduction, giving promising results. However, less work has been dedicated to group 4 transition-metal carbides. Porosoff et al.[10] have shown low activity for TiC compared to that of MoC and Mo_2C, linking that to a high oxygen binding energy, which hinders the catalytic cycle on TiC surfaces. Nevertheless, Quesne et al.[14,15] obtained interesting work function and d-band center values for TiC and ZrC surfaces, which can be correlated with the surface ability to catalyze reduction reactions. Moreover, CO_2 shows significant bond elongation and charge transfer upon adsorption on these materials, suggesting the possibility of catalyzing a reduction reaction.

In this study, TiC and ZrC were therefore chosen for a thorough investigation of their catalytic activity toward CO_2 dissociation and hydrogenation upon their three lowest Miller index surfaces. The investigation was carried out through the density functional theory (DFT) modeling of each of the (001), (011), and metal-terminated (111) surfaces of the two materials, with the aim of identifying the most energetically efficient pathways for the formation of CO, HCOOH, CH_3OH, and CH_4 from carbon dioxide and molecular hydrogen and to identify the critical factors controlling their activity and selectivity. The two carbides and their respective surfaces were identified following previous work on groups 4 and 5 transition metals, which gave promising results for surface properties as well as for CO_2 and H_2 adsorption,[14−16] despite the high surface energy of the (111) surfaces.[14,17]

■ COMPUTATIONAL METHODS

All calculations reported in this work were performed within the framework of the periodic density functional theory using the VASP code (Vienna ab initio software package) version 5.4.1.[18] Core electrons were described using the projected-augmented wave (PAW) method,[19] whereas a plane-wave basis set has been used to expand the valence electron density. The Perdew−Burke−Ernzerhof (PBE) functional[20] was used to approximate exchange and correlation interactions in the framework of generalized gradient approximation (GGA). Additionally, long-range-dispersive interactions were modeled using the Grimme D3 dispersion method.[21] All energies are converged within a cutoff of 520 eV and an electronic self-consistent field (SCF) threshold of 10^{-5} eV. Convergence was determined using the tetrahedron method, implementing Blochl corrected smearing.[22] A dipole correction was enabled in all directions to avoid numerical problems with the perpendicular dipole inherent in the (111) facets. All parameters were benchmarked to optimize computational time and accuracy for the calculations.

The surfaces of the transition-metal carbides (TMCs) studied in the present work were simulated by six atomic layers within (2 × 2) supercell slab models, cutting the bulk along the (001), (011), and (111) planes, as previously reported by Quesne et al.[14] Hence, each slab surface model has 6 atomic layers and 16 atoms per layer. The (001) and (011) surfaces are created so that they preserve bulk stoichiometry, resulting in an equal number of carbon and metal atoms being exposed to the vacuum. Conversely, the (111) plane is parallel to carbon and metal atomic layers, resulting in two possible surface terminations that, respectively, expose carbon and metal atoms to the vacuum in such a way that the stoichiometry is preserved. Such a protocol has been previously applied to TMCs and has been shown to describe accurately the electronic and structural properties of the (111) surfaces and is consistent with previous reports of the same materials.[14] To avoid interactions along the axis perpendicular to the surface, the lattice parameter was increased by 12 Å in such a direction. A 5 × 5 × 1 **k**-points reciprocal lattice matrix was generated using the Monkhorst−Pack method. These parameters were benchmarked, ensuring that vacuum spacing, grid **k**-points, and cutoff energy values allowed convergence to a constant value of the energy. Spin polarization was allowed for the determination of the energy of all structures except for the H_2 reference molecule. Atomic charges were calculated for specific systems through a Bader charge analysis. The energy of the system was minimized by keeping the cell parameters fixed at their bulk-optimized value and allowing relaxation of all atoms excepting those belonging to the two bottom layers of the model slab, which were kept fixed. The minimum energy structures were found using a built-in DIIS algorithm with a convergence force threshold of 10^{-2} eV/Å. The energies of molecular H_2, CO_2, CO, O_2, HCOH, HCOOH, CH_3OH, and CH_4 have been used as references for the adsorption and desorption energies on transition-metal carbide slabs, using half of the energy of the H_2 and O_2 molecules as a reference for atomic H and O adsorption. These calculations have been performed using a single $\mathbf{\Gamma}$ **k**-point and the same cutoff energy as all other calculations within a suitable unit cell, optimized so as to minimize the interaction between neighboring images.

The electronic energies thus calculated were used to compute the reaction and activation energies of the reaction path from CO_2 to its reduced products, which we consider sufficient to inform our understanding of the mechanistic aspects, which is the main objective of this study. Transition-state structures were primarily located using the built-in CI-NEB (climbing image nudged elastic band) algorithm of the VASP code; these calculations used a variable number of system images, in the range 8−13, connected by springs, and was usually performed in two steps: the first was to find an initial guess of the minimum energy path between reactants and products by relaxing the full string of connected images, while the second aimed at identifying the saddle point by turning on the climbing image algorithm on the highest energy image. In the few cases in which the saddle point of the potential energy surface (PES) proved difficult to isolate using this method, an additional third step was used, employing the built-in Dimer method algorithm on the closest NEB image to obtain the relevant transition-state structure. All presented transition-state structures were confirmed to be PES saddle points through a vibrational frequency calculation limited to

https://doi.org/10.1021/acs.jpcc.1c10180
J. Phys. Chem. C 2022, 126, 5138−5150

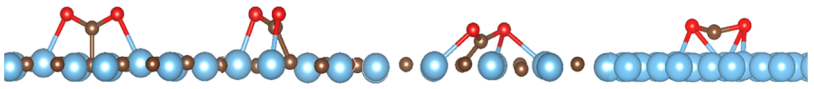

Figure 1. CO_2 adsorption sites on TiC. From left to right: $C_{on\text{-}top}$ on (001), M_2C on (001), M_4C on (011), and M_5 on (111). The same adsorption sites are also found on ZrC(001). The color scheme is as follows: Ti, blue; C, brown; and O, red.

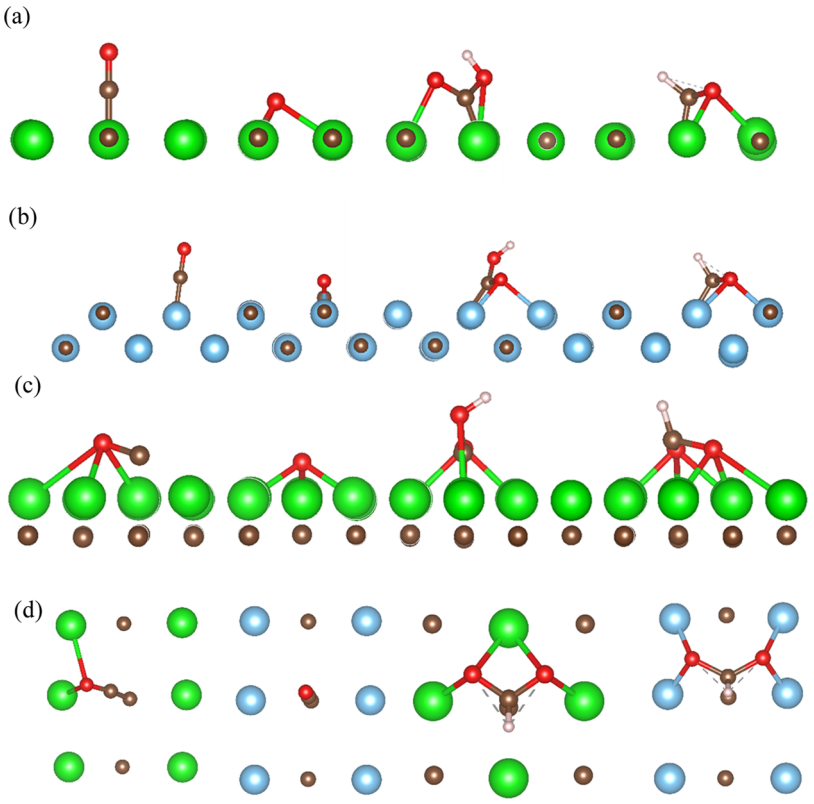

Figure 2. Most favorable adsorption geometries of, from left to right, CO, O, COOH, and HCOO on (a) ZrC(001), (b) TiC(011), and (c) Zr-terminated ZrC(111). (d) Top view, added for clarity, of (from left to right) CO on TiC(011), CO on ZrC(011), HCOO on ZrC(001), and HCOO on TiC(011). Analogous geometries are found for all species not shown in this picture, except for HCOO on ZrC(011), which spontaneously dissociates upon adsorption. The adsorption geometries shown here are those with the minimum energy among those tested on each surface. The color scheme is as follows: Ti, blue; Zr, green; C, brown; O, red; and H, pink.

the adsorbed species and their respective adsorption sites on the surface.

In analyzing the reduction path of CO_2, the key quantities are the adsorption energy (E_{ads}), overall reaction energy (E_r), reduction step energy (E_s), and the activation energy (E_a), which are defined as follows:

Adsorption energy (E_{ads}):

$$E_{ads} = E_{slab+mol} - \left(E_{slab} + \sum E_{mol}\right) \quad (1)$$

The adsorption energy is defined in terms of $E_{slab+mol}$, the total electronic energy of an adsorbed chemical species on a surface, E_{slab}, the energy of the bare surface, and E_{mol}, the electronic energy of the respective isolated molecule(s).

Overall reaction energy (E_r):

$$E_r = E_{stage} - \left(E_{slab} + nE_{CO_2} + m\frac{1}{2}E_{H_2}\right) \quad (2)$$

The overall reaction energy of stage n is defined as the difference between its total electronic energy (E_{stage}) and the sum of the electronic energies of its respective surface and gas-phase molecular reactants in terms of CO_2 and H_2.

Single-step energy (E_s):

$$E_s = E_{stage(n)} - E_{stage(n-1)} \quad (3)$$

The reduction step energy of each stage is instead the energy difference between two subsequent intermediates or products along any reduction path.

Activation energy (E_a):

$$E_a = E^{TS} - E_{stage(n-1)} \quad (4)$$

For a given elementary step, the activation energy is the total energy difference between the identified transition-state structure and the previous stable intermediate.

Each one of the reaction steps and transition states reported in this paper is the result of geometrical optimizations which included distinct initial geometries or reaction coordinates, so that the minimum energy products and reaction paths could be identified for each investigated step. In the case of hydrogenation reactions, molecular hydrogen was always considered to be dissociatively adsorbed on the catalytic surfaces prior to the reaction, consistently with a Langmuir−Hinshelwood mechanism. This choice is consistent with the results of previous works,[16,23] which highlighted small or nonexistent activation barriers for hydrogen chemisorption on the TiC(001) surface and even greater chemical driving force for

https://doi.org/10.1021/acs.jpcc.1c10180
J. Phys. Chem. C 2022, 126, 5138−5150

dissociative adsorption on all other investigated surfaces. Other hydrogenation mechanisms were therefore not investigated.

RESULTS AND DISCUSSION

The investigation of the CO_2 reduction on TiC and ZrC surfaces was carried out in two steps. Initially, the first CO_2 reduction step is analyzed through the three reaction pathways leading to adsorbed CO + O, COOH, and HCOO; the reaction and activation energies of the three reactions are investigated on each of the six surfaces, and the most favorable reaction pathways are identified on each surface. Subsequently, the identified pathways are investigated until the final reduced products, highlighting the activity and selectivity of each surface for the conversion of CO_2 to CO, HCOOH, CH_3OH, and CH_4.

Oxidized and Reduced Carbon on TiC and ZrC Surfaces. The electronic and geometrical effects of CO_2 adsorption are very similar on TiC and ZrC. All surfaces of TiC and ZrC show a favorable chemisorption of CO_2. The molecule is strongly bound to a surface carbon atom on (001) and (011) surfaces, on which all results are comparable to the previously reported computational work on the same surfaces[15] and show similar adsorption patterns as those highlighted on Ti_2C MXenes.[24,25] The main CO_2 adsorption geometries identified for these surfaces, $C_{on\text{-}top}$ for (001) surfaces and M_2C and M_4C on (011) surfaces, are displayed in Figure 1. On the two (111) surfaces, however, we find an adsorption geometry that has not been previously reported: upon adsorption, the CO_2 molecular plane is almost parallel to the plane of the surface, with the two oxygen atoms coordinating 5 metal atoms in the M_5 adsorption site. Longer bond lengths and more reduced CO_2 molecules are found, as the bond elongates up to +0.3 Å compared to the gas-phase molecule and the CO_2 carbon atom gains +1.8 *e* of charge, but the adsorption is less exothermic than on the (011) surfaces, as E_{ads} is computed to be of −3.1 eV on TiC(111) and of −3.2 eV on ZrC(111). Previous studies[15] only reported vertical adsorption sites for these surfaces, which show significantly less exothermic adsorption. As can be seen in Figure 1, all four identified adsorption sites have a bent geometry.

In the initial step of the catalytic reduction process, CO_2 may either dissociate yielding CO and O on the surface of the carbide or be hydrogenated at the C or O atoms, yielding, respectively, a carboxyl or a formate on the catalyst surface. In the latter case, the hydrogen atom is transferred from the surface of the catalyst since the dissociation of the H_2 molecule has previously been shown to be spontaneous in all but the most unfavorable conditions.[16] These first reaction steps have been investigated on all surfaces, modeling the formation of the three first-step intermediates

$$CO_2 \rightarrow CO + O \quad (a)$$

$$CO_2 + 1/2H_2 \rightarrow COOH \quad (b)$$

$$CO_2 + 1/2H_2 \rightarrow HCOO \quad (c)$$

The adsorption of each of the chemical species on every surface has therefore been studied, identifying the minimum energy structures shown in Figure 2 and highlighting the adsorption energies reported in Table 1. The adsorption of CO is generally very exothermic (E_{ads} = −1.82 to −3.91 eV) on all surfaces. $C_{on\text{-}top}$ sites are dominant on both (001) surfaces, as shown by Figure 2a, in which the molecule stands almost perpendicular to the plane of the catalyst, only slightly leaning toward a metal atom; on these sites, the C−O bond shows significant elongation (increasing to 1.20 Å), as the distance between the adsorbed molecule and the nearest surface carbon atom also resembles that of a strong covalent C−C bond at 1.32 Å. The (011) surfaces lead to the most exothermic CO adsorption on both carbides, as was previously noted for the case of CO_2; Figure 2b shows the most favorable adsorption site on TiC(001), where the CO molecule is roughly perpendicular to the surface and coordinated only through the carbon atom. While a similar adsorption is also possible on ZrC(011), a more exothermic adsorption site is present, in which the CO molecule is roughly parallel to the surface and coordinates a surface carbon with its carbon atom and two metal atoms with is oxygen atom; on both surfaces, the molecule appears to be activated, as shown by the elongation of the C−O bond, which reaches 1.27 Å on ZrC(011). Both adsorption sites are shown in Figure 2d.

Table 1. Adsorption Energies for CO, O, COOH, and HCOO on TiC and ZrC, Given in eV[a]

	CO	O	COOH	HCOO
		TiC		
(001)	−1.82 ($C_{on\text{-}top}$)	−2.54 (M_2C)	−1.25 (M_2C)	−2.08 ($C_{on\text{-}top}$)
(011)	−3.22 ($C_{on\text{-}top}$)	−4.40 (M-O-C)	−1.82 (M_4C)	−5.35 (M_4C)
(111)	−3.22 (M_2)	−5.76 (M_3)	−1.20 ($M_{4\text{-}vertical}$)	−6.12 ($M_{5\text{-}up}$)
		ZrC		
(001)	−2.13 ($C_{on\text{-}top}$)	−2.79 (M_2C)	−1.70 (M_2C)	−3.29 ($C_{on\text{-}top}$)
(011)	−3.91 (C-M_{bridge})	−4.56 ($M_{2\text{-}bridge}$)	−3.74 ($C_{on\text{-}top}$)	N/A
(111)	−3.13 (M_2)	−5.85 (M_3)	−2.46 ($M_{4\text{-}vertical}$)	−6.17 ($M_{5\text{-}up}$)

[a]Only the most favorable adsorption sites are considered in this table.

The (111) surfaces offer multiple coordination patterns, resulting in low energy structures where both atoms of CO maximize coordination by lying almost parallel to the surface, as shown in Figure 2c. Isolated oxygen atoms are bound very strongly to all surfaces (E_{ads} = −2.5 to −5.9 eV), as expected from the well-known tendency of TMCs to form oxycarbides.[26] On the (001) surfaces, adsorbed O is coordinated to one carbon and two metal atoms. On the (011), oxygen interacts very strongly with carbon atoms, pulling them strongly out of the plane of the surface, whereas on the (111), O fits in the hexagonal sites coordinating three metal atoms, binding strongly to the surface.

The carboxyl group formed by the hydrogenation of CO_2 on one of the oxygen atoms also has different optimized geometries on the different surfaces. On both (001) surfaces, two planar structures could be identified: the first, named as $C_{on\text{-}top}$ adsorption site, has its O−C−O plane perpendicular to the surface and is slightly bent to maximize the interaction between the nonhydrogenated oxygen and the surface; alternatively, the second structure, the M_2C adsorption site, is bent toward the surface to maximize the interaction between the latter and the oxygen atoms. The two structures have very similar energies (ΔE_{ads} < 0.05 eV), with the latter at a slightly lower energy, which is shown in Figure 2a. On the (011), similar structures are found albeit with different relative stabilities, with $C_{on\text{-}top}$ being stable on ZrC, while the M_2C adsorption site is favored on TiC. On the (111) surface of both

https://doi.org/10.1021/acs.jpcc.1c10180
J. Phys. Chem. C 2022, 126, 5138−5150

carbides, the COOH group is most stable when aligned perpendicularly to the surface, with C═O coordinated to the surface and −OH pointing upwards.

Formate groups formed by the hydrogenation of a CO_2 carbon atom are not stable on ZrC(011), giving spontaneous dissociation to an sp^2-hybridized HCO on a $C_{on\text{-}top}$ site, with O coordinated to a metal, plus adsorbed oxygen. The same process was expected for TiC(011), but in this case, a surface formate intermediate could be isolated, as shown in Figure 2b. On the four other surfaces, HCOO has stable configurations similar to those for COOH, with $C_{on\text{-}top}$ and M_5 being the most favored on (001) and (111) surfaces, respectively, on both carbides.

Across the three surfaces, adsorption shows similar characteristics for TiC and ZrC, as adsorption geometries and energies are similar on the two materials for the (001) and (111) surfaces, where adsorption geometries are always equivalent, with only minor differences due to the change in lattice parameters between the two cells. In contrast, all adsorption sites identified for the (011) surfaces differ between the two materials. Energetically, adsorption on ZrC is always shown to be more exothermic than the equivalent adsorption on TiC; the energy difference is usually small (0.02−0.35 eV) but exceeds 1 eV for HCOO/(001), COOH/(011), and COOH/(111).

CO_2 Dissociation and Hydrogenation. As we have seen, the species discussed above are all adsorbed exothermically. However, when we consider the energetics of reactions 1−3 above, we find that the energy of the reaction step on the surface is only negative for the dissociation reactions, while it can be significantly positive for the two hydrogenation pathways.

Table 2 summarizes the reaction energies associated with the formation of CO, COOH, and HCOO, reported with respect to gas-phase CO_2 (+ 1/2 H_2 in the case of hydrogenation) and to the single reaction step from adsorbed CO_2. As noted, the dissociation reactions are the only ones for which single-step energies are negative, due to the high adsorption energies found for CO and O, which bind strongly to the surfaces of TiC and ZrC. However, previous reports[8,10] have shown that when oxygen is bound too strongly, it can hinder the catalytic cycle. In contrast, single-step reaction energies for the formation of COOH and HCOO are generally endothermic, as a result of the relative instability of these intermediates. Nevertheless, the reaction energies from gas-phase reactants are generally exothermic, the formation of HCOO on the TiC(001) surface being the only exception, for which E_r = +0.19 eV. As a result, it is possible that the adsorption of CO_2 and H_2 on the low-index surfaces of TiC and ZrC might provide the energy for the formation of these intermediates on the catalysts, especially if an Eley−Rideal type of mechanism is operative.[27] The endothermicity of CO_2 hydrogenation can also be linked to the results of hydrogen adsorption on TMCs[16] since hydrogenation on TiC and ZrC surfaces is always exothermic but energy is required for the formation of HCOO and COOH, as one strongly bound H atom has to be removed from binding directly to the surface. On the (011) and (111) surfaces, because of their more exothermic adsorptions, this results in especially high single-step energies for COOH formation. HCOO formation, however, is less thermodynamically unfavorable on the (111) surfaces, owing to the very strong bond between this intermediate and the surface.

Table 2. Reaction Energies and Single-Step Energies (in eV) for the Dissociation to CO + O, Hydrogenation to COOH, and Hydrogenation to HCOO[a]

	CO + O		COOH		HCOO	
	E_r	E_s	E_r	E_s	E_r	E_s
			TiC			
(001)	−1.13	−0.23	−1.25	0.59	0.19	2.03
(011)	−7.05	−3.6	−3.38	1.43	−3.38	1.43
(111)	−5.70	−2.60	−2.76	1.43	−3.84	0.35
			ZrC			
(001)	−1.72	−0.04	−1.70	0.95	−1.02	1.63
(011)	−5.03	−0.84	−3.73	1.71	−5.92*	−0.48*
(111)	−5.67	−2.49	−2.47	1.91	−3.9	0.48

[a]For each reaction, two energies are reported, differing for the reference used: in the column on the left of each section, the reaction energy E_r is reported, which is the energy of the intermediate on the surface of the catalyst minus the energy of the gas-phase reactants and pristine surface; in the column on the right of each section, the single-step energy E_s is reported, which is the energy of the intermediate on the surface of the catalyst minus the energy of the previous intermediate on the same surface. The energies reported for HCOO on ZrC(011) are marked with an asterisk because they are referred to the formation of HCO + O since HCOO dissociation occurs spontaneously on this surface.

From the results of Table 2, it is also possible to make a preliminary assessment of how the three competitive reactions are balanced on each surface. In absolute terms, the dissociation is always thermodynamically favored, as it always shows $E_s < 0$ for the single-step process. However, if only the hydrogenation reactions are considered, a strong preference toward the formation of COOH is found on (001) surfaces, while on (111) surfaces, the preference is toward the formation of HCOO, which on TiC(111) has the least positive single-step reaction energy of all hydrogenated intermediates. On the two (011) surfaces, the formate is unstable and can dissociate spontaneously to CHO + O. It was possible to identify a formate intermediate on TiC(011), for which E_s = 1.43 eV, the same as for CO_2 hydroxylation. On ZrC(011), however, HCOO is so unstable that it undergoes spontaneous dissociation and no intermediate could be found. Table 2 reports E_s = −1.48 eV for this reaction, which refers to the formation of CHO + O.

To evaluate the selectivity of each surface, the simple prediction of reaction energies is insufficient. Nudged elastic band calculations (NEB and CI-NEB) and the dimer method have been employed to sample the region of the potential energy surface connecting each intermediate to their adsorbed reactants, identifying the transition states corresponding to the reactions leading to CO, COOH, and HCOO on (001), (011), and (111) surfaces. From this investigation, two reactions have been excluded: the formation of formate on TiC(001) and ZrC(001) has been considered too high in energy to take place, the former showing the only positive reaction energy from gas-phase reactants, the latter being strongly unfavorable compared to COOH formation. Figure 3 illustrates the initial state, transition state, and final state of the PES linking adsorbed CO_2 and H to COOH on TiC(001), CO_2 to CO and O on ZrC(011), and CO_2 and H to HCOO on TiC(111). The calculated data for those and all other reactions are reported in Table 3.

https://doi.org/10.1021/acs.jpcc.1c10180
J. Phys. Chem. C 2022, 126, 5138−5150

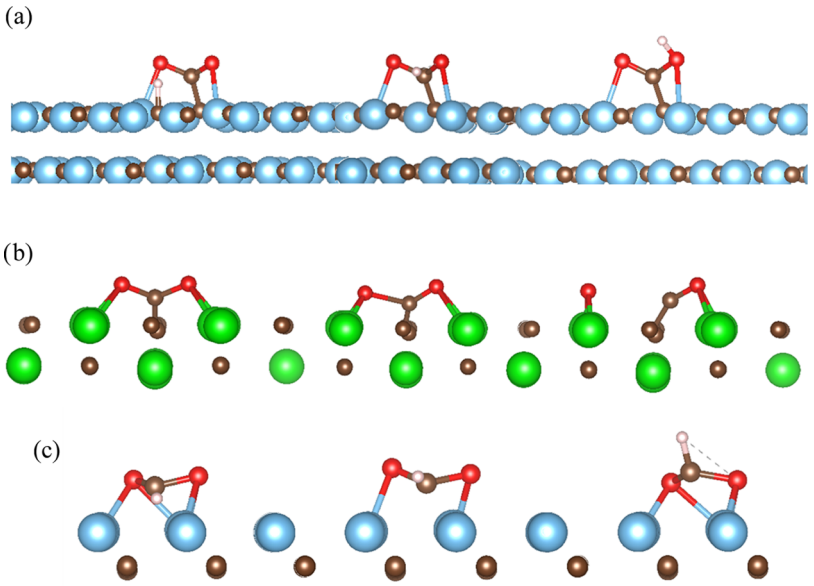

Figure 3. Proposed reduction mechanism of (a) CO_2 hydrogenation to COOH on TiC(001), (b) CO_2 dissociation to CO + O on ZrC(011), and (c) CO_2 hydrogenation to HCOO on TiC(111). From left to right: initial state, in which the reactants are adsorbed on the surface of the catalyst; transition state, identified through the presence of one imaginary frequency related to the formation of the desired product; and final state, in which the product is adsorbed on the surface of the reactant. The color scheme is as follows: Ti, blue; Zr, green; C, brown; O, red; and H, pink.

Table 3. Activation and Reactive Step Energies of CO_2 Reduction over TiC and ZrC[a]

	E_{ads}	E_a	E_s
	TiC		
001—CO	−0.90	+2.13	−0.23
011—CO	−3.45	+0.69	−3.6
111—CO	−3.11	+0.99	−2.60
001—COOH	−1.84	+1.58	+0.59
011—COOH	−4.80	+2.15	+1.43
111—COOH	−4.19	+2.15	+1.43
001—HCOO	−1.84	N/A	+2.03
011—HCOO	−4.80	+1.39	+1.43
111—HCOO	−4.19	+1.44	+0.35
	ZrC		
001—CO	−1.68	+1.86	−0.04
011—CO	−4.19	+0.49	−0.84
111—CO	−3.18	+1.29	−2.49
001—COOH	−2.65	+1.48	+0.95
011—COOH	−5.44	+1.97	+1.71
111—COOH	−4.38	+2.44	+1.91
001—HCOO	−2.65	N/A	+1.63
011—HCOO	−5.44	>3 eV	−0.48*
111—HCOO	−4.38	+1.58	+0.48

[a]All energies are referred to the adsorbed CO_2, for dissociation reactions, or CO_2 + H, for hydrogenation reactions, and are reported in eV. The first column refers to the adsorption energy; the second row is the activation energy, hence, the energy difference between the adsorbed reactant and the transition state; the final row reports the energy of the products referred to that of the adsorbed reactants.

Dissociation to CO on both (001) surfaces is mildly exothermic but shows very high barriers—over 2 eV for TiC(001). These results might seem inconsistent with the previous investigation of CO_2 adsorption on the same surfaces,[15,28] which highlight the efficient activation of the CO_2 molecule on the (001) surfaces of several transition-metal carbides through the investigation of their elongated bond distances, modified bond angle, and effective charge transfer from the surface to the carbon center. The calculations presented here suggest that this discrepancy is due to an inefficient coordination of the transition state correlated to the dissociation of the C−O bond, since the electronic and geometric characteristics of adsorbed CO_2 that indicate activation of the molecule[28] do not translate into a sufficiently low activation barrier.

This result shows how, even if the (001) surface can chemisorb both reactants and products efficiently, CO_2 is not sufficiently activated on these surfaces for appreciable dissociation to occur. CO_2 adsorbed on TiC(001) and ZrC(001) shows longer bond lengths, a bent geometry, and a higher number of electrons than the gas-phase molecule, all characteristics that have been correlated with CO_2 activation.[29] However, this activation is ineffective for this reaction since on both carbides, the transition state has a higher energy than the gas-phase reactants, effectively ruling out the direct dissociation of CO_2 on (001) surfaces.

The dissociation reaction is considerably more exothermic on (011) and (111) surfaces, as the more exposed metal atoms can coordinate CO_2 more efficiently while the C−O bond is elongated until full dissociation. Dissociation on ZrC(011) is, of all reactions, the one with the lowest energetic barrier (E_a = 0.49 eV over the adsorbed reactants), while TiC(011) shows the most exothermic reaction energy (E_s = −3.60 eV) but has a slightly higher activation barrier, E_a = 0.69 eV. This can be correlated with the higher metal area exposed on ZrC, allowing for a better coordination of the dissociating oxygen but resulting in its less efficient coordination once the reaction is complete. However, this trend is inverted for the transition states on (111) surfaces: as a result of the larger cell parameters of ZrC, the dissociating oxygen cannot be coordinated as efficiently, resulting in a higher barrier than that on TiC(111).

Conversely, the hydrogenation reaction to carboxyl is most favorable on the (001) surfaces of TiC and ZrC. In all cases, the reaction step is endothermic, and the barrier is at least 1.5

https://doi.org/10.1021/acs.jpcc.1c10180
J. Phys. Chem. C 2022, 126, 5138−5150

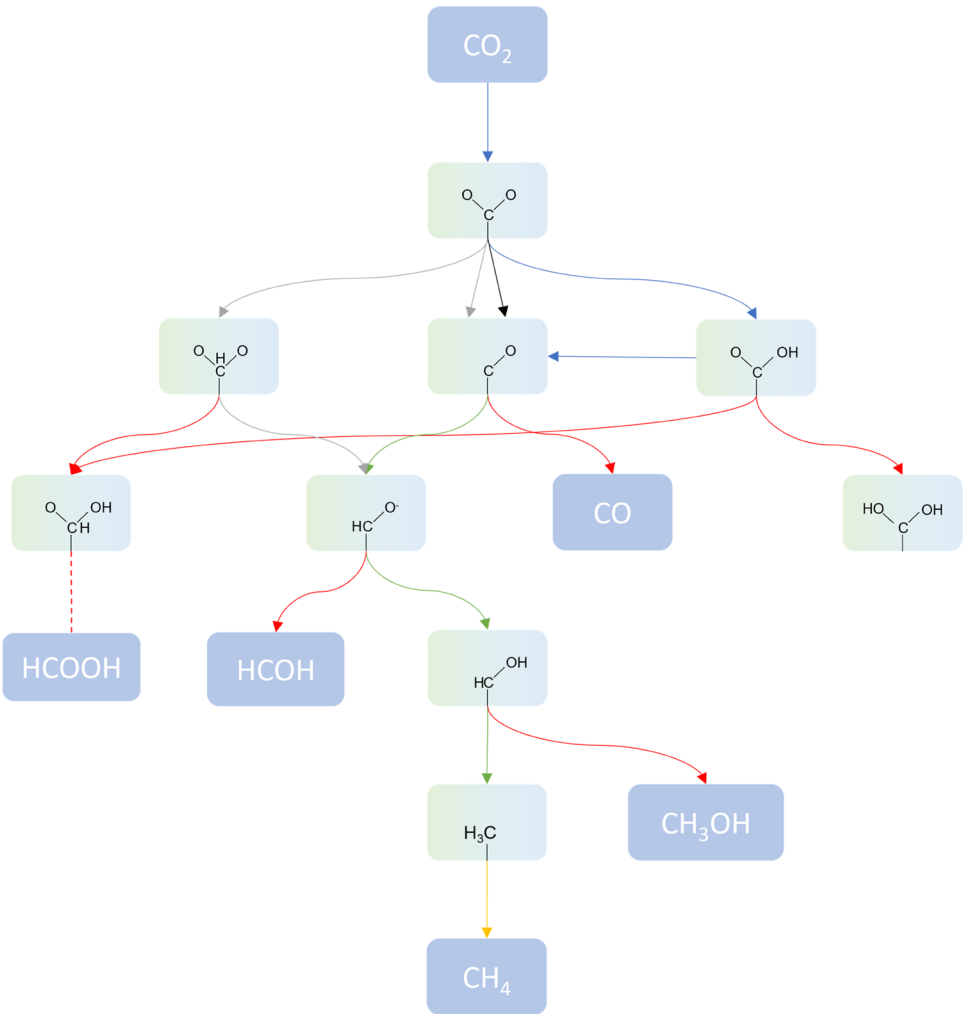

Figure 4. Proposed reduction pathways of CO_2 on transition-metal carbide surfaces. The background chosen for each compound corresponds to its phase: dark blue for gas phase, and green and light blue for molecules on TiC and ZrC, respectively. The color code of the arrows between each compound is associated with the results of the present investigation: blue for reactions favored on (001) surfaces, black for (011), gray for (111), green for reactions favored on all surfaces, red for reactions hindered by either thermodynamic or kinetic impediments, and yellow for desorption reactions. As will be discussed in this paper, the main reduction path on all surfaces is that leading to CH_4 through a HCO intermediate.

eV above the adsorbed state of the reactants. However, this energy can be provided by the adsorption energies of CO_2 and H_2 on the surfaces of the catalysts, as both are significantly larger than the activation barriers. This reaction is thermodynamically least unfavorable on TiC(001), where it shows an E_s = +0.59 eV, while kinetically ZrC shows a slightly lower barrier of E_a = +1.48 eV. The hydrogenation on both (011) and (111) surfaces is instead significantly endothermic and shows barriers of 2 eV and higher, hindering the formation of COOH on these four surfaces. As mentioned in the previous section, the strong bond formed by hydrogen with these surfaces can be considered as a reason for the high hydrogenation barriers found on this surface.

The hydrogenation to formate presents an interesting case study, as the results vary greatly depending on the surface. On the (001) surfaces, as mentioned in the previous section, the reaction is highly endothermic and no investigation of the potential energy surface has been performed. On the two (011) surfaces, formate can dissociate rapidly to HCO + O. The process seems to be spontaneous on ZrC, for which no HCOO intermediate could be isolated, while it requires a small activation energy on TiC. This reaction is more viable than the hydrogenation to carboxyl despite its identical reaction energy, as E_a(HCOO) = 1.47 eV < E_a(COOH) = 2.44 eV. On ZrC(011), however, the structure of the transition state leading to the simultaneous hydrogenation and dissociation is found to be very close to the unstable intermediate HCOO, which obviously leads to a high kinetic barrier (E_a > 3 eV) after which the intermediate spontaneously dissociates. The height of this barrier rules out the possibility of hydrogenation to formate on the latter surface, as it is significantly higher than E_a = 1.97 eV found for carboxyl production. Conversely, on both (111) surfaces the reduction to formate is mildly endothermic, with E_s = 0.35 eV on TiC, probably due to the geometry of the surfaces, which allows for strong interaction of the carbon and oxygen atoms of HCOO with the metal atoms of the material while minimizing interaction with hydrogen. Activation barriers on the two surfaces are similar—E_a(TiC) = 1.44 eV, E_a(ZrC) = 1.58 eV. While the kinetic barrier to hydrogenation is high, it is still much lower than the adsorption energies of the reactants, CO_2 and H_2; it should therefore be possible to observe the COOH intermediate if the two reaction steps take place in such a way that the energy required to overcome the

https://doi.org/10.1021/acs.jpcc.1c10180
J. Phys. Chem. C 2022, 126, 5138−5150

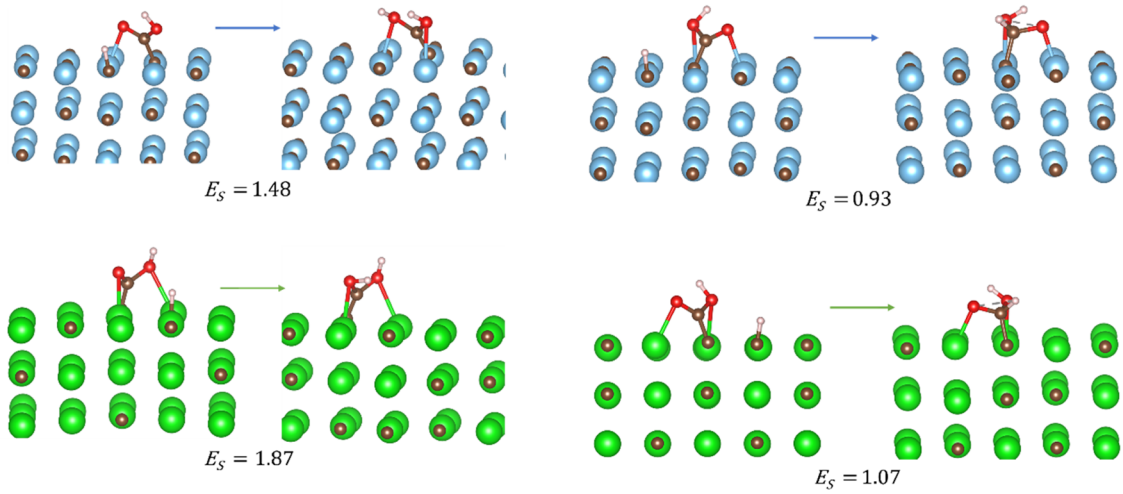

Figure 5. TiC (top) and ZrC (bottom) (001) surface-mediated formation of dihydroxymethylidene (left) and formic acid (right). All energies are given in eV.

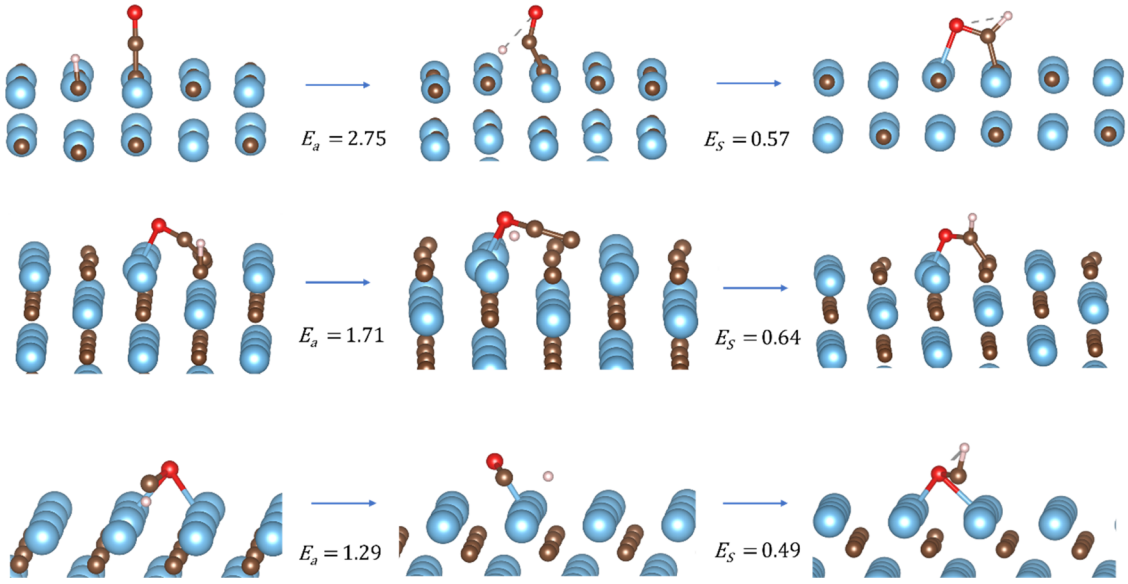

Figure 6. Surface-mediated HCO formation by TiC by (top) (001), (middle) (011), and (bottom) (111)-metal-terminated facets. All energies are given in eV related to surface-bound carbon monoxide and hydrogen.

barrier to hydrogenation is provided by the adsorption onto the (111) surfaces.

Surface-Mediated Product Selectivity. After the first reduction step, multiple pathways are available for the conversion of CO_2 into useful chemicals, as illustrated in Figure 4. The results highlighted in the first part of the present work allowed us to reduce the number of investigated surfaces for the subsequent reaction steps by excluding those involving high activation energies. The final part of our study will investigate, first, the reaction steps following the dissociation to CO on the (011) and (111) surfaces, and second, those following the hydrogenation to COOH on the (001) and HCOO on the (111) surfaces. All other reaction paths, as discussed above, have been discounted due to the high energies of their intermediate steps or transition states, which inhibit further reaction.

The investigation of the second steps of the reaction has entailed the analysis of the thermodynamic reaction energies of the pathways for the conversion of COOH and HCOO to HCOOH on the (001) and (111) surfaces, respectively; COOH to CO on (001) surfaces; and CO to HCO and COH on (011) and (111) surfaces. On the (111) surface of TiC, all attempts at optimizing HCOOH led to its decomposition to HCO and OH. It was therefore concluded that all reactivity would proceed via HCO rather than via HCOOH. The alternative ZrC(111) facet does enable the formation of a stable HCOOH intermediate. However, despite the negative reaction energy of $E_r = -0.51$ eV, this step is strongly endothermic, with $E_s = 3.4$ eV with respect to HCOO. Such an endothermic reaction energy will be inaccessible, and therefore formic acid is also ruled out as a final product on the ZrC(111) surface.

To assess the viability of COOH hydrogenation on the (001) facets of TiC and ZrC, the reaction landscapes for the transfer of a surface hydrogen to either oxygen atom or to the carbon center were computed. Figure 5 shows the driving force for the production of dihydroxymethylidene and formic acid from COOH on the (001) surfaces of TiC and ZrC. The

https://doi.org/10.1021/acs.jpcc.1c10180
J. Phys. Chem. C 2022, 126, 5138−5150

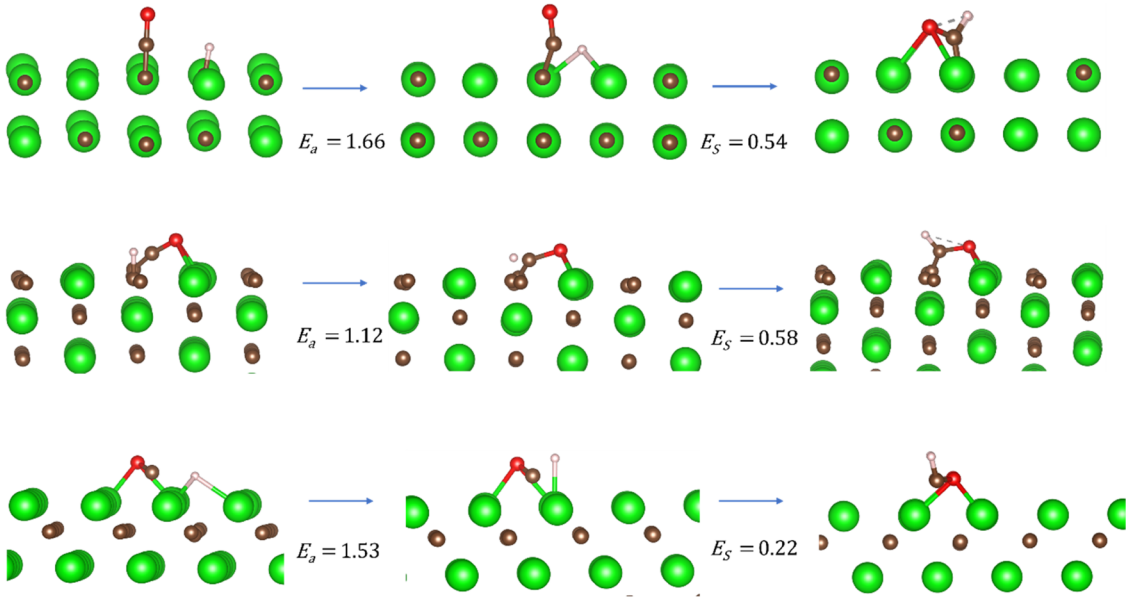

Figure 7. Surface-mediated HCO formation by ZrC by (top) (001), (middle) (011), and (bottom) (111)-metal-terminated facets. All energies are given in eV related to surface-bound carbon monoxide and hydrogen.

reaction energy for the formation of dihydroxymethylidene is far too high for it to be an important intermediate in the further reduction of COOH and was not considered further. Similarly, a second hydrogenation of the hydroxyl oxygen followed by the dissociation of the product into CO and H_2O is shown to be highly endothermic, with E_s = 1.67 eV on TiC(001) and E_s = 1.99 eV on ZrC(001).

While still endothermic, the reaction energy for formic acid formation (∼1 eV) appears to be more accessible, so CI-NEB calculations were undertaken to determine the activation energies for such a reaction. Unfortunately, the results showed that these pathways were kinetically blocked by barriers larger than 2 eV. The direct formation of formic acid was therefore ruled out as a possible outcome of the CO_2 reduction upon these catalysts. As a result, the investigation shifted toward the hydroxylation of surface-bound CO/HCO intermediates, as the most likely reaction paths for carbide-catalyzed CO_2 reduction.

Our calculations suggest that the most likely route for the CO/HCO intermediates on both (001) facets was the surface-mediated decomposition of COOH to CO and OH. It was determined that such a decomposition corresponds to a decrease in energy of E_s = −0.70 eV on the ZrC(001) facet but was slightly endothermic on the TiC(001) surface (E_s = +0.21 eV). Nevertheless, both reaction steps can be considered accessible when considering both the potential gain in entropy as COOH is dissociated and the inherent margin of error of the calculated energies. Therefore, it might be expected that COOH readily decomposes on the (001) termination of ZrC and COOH/CO + OH forms an equilibrium on the (001) surface of TiC, which is then pushed toward the decomposed product as CO goes through further reduction. For completeness, the decomposition of formate (to HCO + O) was also considered, obtaining reactive step energies of E_s = +0.46 eV and E_s = +1.02 eV on the (001) surfaces of TiC and ZrC, respectively. Calculations discussed below examining CO hydrogenation will indicate that the decomposition of formate might be important as a shortcut to HCO formation on the (001) surface of TiC (see Figure 6). However, carboxylic acid decomposition is likely to be the dominant pathway for the alternative ZrC(001) facet.

Data from Figure 6 show that the most active surface for carbon monoxide hydrogenation to HCO on TiC is the metal-terminated (111) surface, followed closely by the (011) facet. While this ordering is reversed on ZrC, all barriers were assessed to be larger than 1 eV. As mentioned above, an activation barrier of almost 3 eV, such as that found for HCO formation on TiC(001), clearly implicates formate decomposition as a more likely mechanism for HCO formation than CO hydrogenation. Interestingly, these results indicate that surface geometry—and especially CO adsorption morphology—plays a far more significant factor in the activation energies for CO hydrogenation than does hydrogen adsorption, with no obvious correlation between barrier heights and the surface hydrogenation energies previously reported using comparable methodologies.[16] There are far more product-like and higher-energy transition states on the two (001) surfaces, and the fact that the preferred binding site for the hydrogen and carbon atoms are both located on top of a surface carbon site implies that these late transition states are far from optimal. The more favorable barrier seen on the (111) surface of TiC over the comparable facet of ZrC is also due to surface morphology, as the shorter TiC lattice constants enable a transition state where the hydrogen atom is close to a highly coordinated hollow site. The hydrogen position in the comparable ZrC(111) transition state, on the other hand, more closely resembles a $C_{on\text{-}top}$ low-coordinated position, as shown in Figure 7.

Across all surfaces investigated, our calculations have indicated the importance of a common HCO intermediate, either as a result of direct hydrogenation of CO (as is the case for (011) and (111) facets) or via the (001) surface-mediated decomposition of formate or carboxylic acid. It was therefore decided to focus on the further reduction of HCO. Table 4 shows the reaction energies for HCO hydrogenation to formaldehyde. Crucially, the desorption energy for formaldehyde is very high for all surfaces except for TiC(111), where the value for H_2CO release is actually slightly negative

https://doi.org/10.1021/acs.jpcc.1c10180
J. Phys. Chem. C 2022, 126, 5138−5150

Table 4. Activation and Reaction Energies of HCO Reduction over TiC and ZrC[a]

	E_{ads}(HCO)	E_a	E_s
	TiC		
001—H_2CO	−1.81	+1.67	−1.49
011—H_2CO	−4.11	+1.77	−6.78
111—H_2CO	−3.88	+5.60	−0.49
001—HCOH	−1.81	+1.08	−2.12
011—HC OH[b]	−4.11		−5.80
111—HC OH[b]	−3.88		−5.26
	ZrC		
001—H_2CO	−2.25	+5.86	−2.01
011—H_2CO	−4.57	+1.70	−4.51
111—H_2CO	−3.89	+1.43	−3.93
001—HCOH	−2.25	+1.80	−1.89
011—HC OH[b]	−4.57		−5.83
111—HCOH	−3.89	+2.63	−2.85

[a]The first column refers to the surface-bound HCO with reference to gas-phase CO and one-half of H_2 E_{ads}(HCO); the second row is the activation energy E_a, and the third and final row reports the energy of the products referred to that of the reactants E_s. All energies are reported in eV.

(−0.09 eV/mol). Additionally, when examining the transition-state energies of formaldehyde formation, we can rule out that this process takes place on the TiC(111) surface entirely. On this surface, the alternative and highly exothermic oxygen hydrogenation step appears far more likely, but no stable HCOH minima could be found on either (011) surface, with HCOH undergoing a barrierless decomposition to surface-bound HC and OH species.

The decomposition of HCOH is likely to promote the production of various surface-bound C1 hydrocarbons and water, with no obvious route through to methanol formation. However, the strongly bound formaldehyde on the other surfaces does offer the potential for the production of the alcohol product. Therefore, the hydrogenation of H_2CO was examined on all surfaces, with the resulting reaction energies given in Table 5. Hydrogenation of formaldehyde to CH_3O is an essentially thermodynamically neutral process on both (001) surfaces and on the (011) facet of ZrC, while the reaction energy is highly exothermic on both (111) surfaces studied. Importantly, the adsorption energy for surface-bound formaldehyde is far too large to enable the desorption to occur on any of these facets. Interestingly, the reaction energy is highly endothermic on the (011) facet of TiC, which is due to

Table 5. Reaction Energies E_r for H_2CO Reduction to H_3CO and H_3COH over TiC and ZrC[a]

	H_2CO	H_3CO	H_3C + OH
	TiC		
001—H_3C OH	−1.49	−1.74	−2.92
011—H_3C OH	−6.78	−3.98	−8.11
111—H_3C OH	−0.49	−4.78	−6.63
	ZrC		
001—H_3C OH	−2.01	−1.94	−3.33
011—H_3C OH	−4.51	−4.44	−6.39
111—H_3C OH	−3.93	−4.87	−6.17

[a]Due to the lack of a stable CH_3OH intermediate, the last column refers to adsorbed CH_3 and OH species on each surface. All energies are reported in eV.

the bidentate binding of formaldehyde causing an additional σ-bond not seen in the monodentate H_3CO. Most importantly, and despite repeated attempts, no stable methanol species could be produced by hydrogenation of surface-bound H_3CO, and in all cases, decomposition to surface CH_3 and OH species was observed to be a barrierless process. This result opens a new route toward methane and water formation, with the alternative pathway to methanol being again blocked by the surface-mediated cleavage of the C−O bond.

Taken together, these results help to rationalize the observed selectivity toward methane production over methanol when CO_2 conversion by TiC and ZrC is investigated.[10,30] The selectivity that these materials have demonstrated experimentally is here confirmed computationally on all low-index surfaces, as all paths leading to CO and other valuable products are blocked by either endothermic reactions or very high activation energies. Furthermore, the match between experimental and computational results suggests the importance of the HCO intermediate on all facets of ZrC and TiC as a fundamental step in the reduction path for CO_2. The color scheme of Figure 4 shows the favorable and unfavorable reactions on each surface, rationalizing the product selectivity and proposing a few possible reduction paths. These results provide a clearer picture of the reactivity on each facet of the carbides. Figures 8 and 9 combine the reduction paths of CO_2 on the three surfaces of TiC and ZrC, displaying the reaction energies (i.e., the energy of the adsorbed intermediate relative to the appropriate number of CO_2 and H_2 molecules in the gas phase) of each intermediate along the six paths. The reaction landscapes are similar for the two carbides, further revealing the similarity between the catalytic properties of the two materials, and in all cases, the HCO intermediate is central within the reduction path to CH_4. Furthermore, on both materials, the (001) surface presents the least negative energies, suggesting an easier release of CH_4 and a consequently better catalytic activity for these facets, in contrast to previous reports on the hydrogen evolution reaction on the same surfaces,[16] for which the (001) facet appeared to be too stable to catalyze the reaction adequately. On both carbides, however, reported conversion rates are low, probably due to oxidation of the surface under reaction conditions.[10,30] This behavior might be due to the highly negative reaction energies reported in Figures 8 and 9 (−3 to −8 eV), which slow the release of the reduced products, as well as to the strong adsorption of oxygen on the surface, reported in Table 1, which might create a passivating layer at the interface of the catalyst.

SUMMARY AND CONCLUSIONS

This work has reported a systematic study into the selective hydrogenation of carbon dioxide over the low-Miller index (001), (011), and (111) surfaces of TiC and ZrC. DFT calculations and periodic models have been used to assess the viability of reaction mechanisms toward formic acid, carbon monoxide, formaldehyde, methanol, and methane. Carbon dioxide adsorbs very exothermically on all surfaces and is highly reduced (in many cases by the transfer of more than one electron from the carbide), with the highly activated adsorbate readily undergoing further surface-mediated reactions. The C−O bond cleavage appears to be favored on both (011) surfaces, while COOH formation appears to be the initial step on the two (001) facets. The alternate metal-terminated (111) surfaces are capable of catalyzing both carbon monoxide and

https://doi.org/10.1021/acs.jpcc.1c10180
J. Phys. Chem. C 2022, 126, 5138−5150

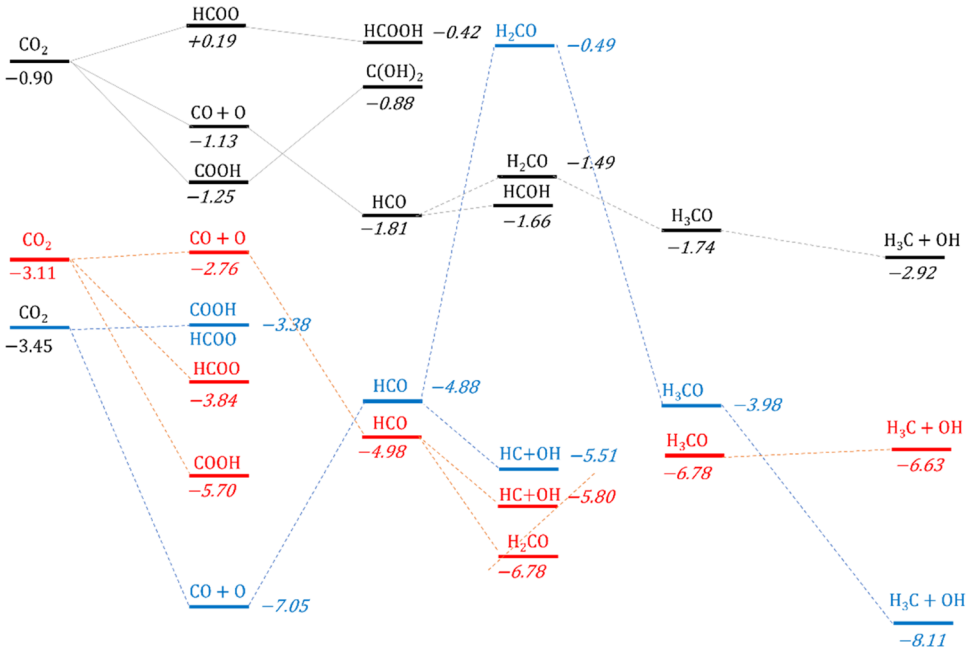

Figure 8. Thermodynamic profile of the reaction paths for CO_2 reduction on TiC (001) (black), (011) (blue), and (111) (red) surfaces. The numbers displayed are the reaction energies of each intermediate (E_s), in eV. All energies are referred to all reactants and products being simultaneously adsorbed on the relevant surfaces, without interaction between the adsorbed species, so that the reference energy level corresponds to two adsorbed hydrogen molecules and gas-phase CO_2 for all steps. Only the carbon-containing molecule of each step is reported for clarity.

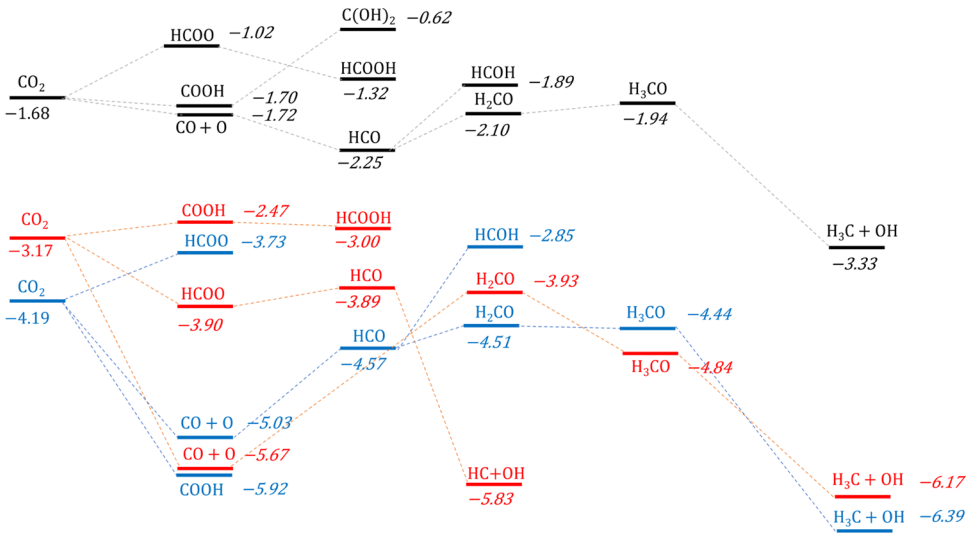

Figure 9. Thermodynamic profile of the reduction paths for CO_2 reduction on ZrC (001) (black), (011) (blue), and (111) (red) surfaces. The numbers displayed are the reaction energies of each intermediate (E_s), in eV. All energies are referred to all reactants and products being simultaneously adsorbed on the relevant surfaces, without interaction between the adsorbed species, so that the reference energy level corresponds to two adsorbed hydrogen molecules and gas-phase CO_2 for all steps. Only the carbon-containing molecule of each step is reported for clarity.

formate production as their primary reaction step. Whichever initial mechanism is promoted, all accessible reduction pathways go through a HCO intermediate and ultimately promote the formation of methane over any other reduction product. These results help to rationalize the experimentally observed selectivity toward methane over carbon monoxide when CO_2 conversion by hydrogen is studied and further demonstrate the difference in chemical reactivity of the three facets of each carbide.

■ ASSOCIATED CONTENT

Supporting Information

The Supporting Information is available free of charge at https://pubs.acs.org/doi/10.1021/acs.jpcc.1c10180.

Activation energy for CO_2 adsorption reported in this work compared to previously reported values[15] (Table S1) (PDF)

https://doi.org/10.1021/acs.jpcc.1c10180
J. Phys. Chem. C 2022, 126, 5138−5150

AUTHOR INFORMATION

Corresponding Author

Fabrizio Silveri − *School of Chemistry, Cardiff University, Cardiff CF10 3AT, U.K.; Departament de Ciència de Materials i Química Física and Institut de Química Teòrica i Computacional (IQTCUB), Universitat de Barcelona, 08028 Barcelona, Spain; Gemmate Technologies s.r.l., 10090 Buttigliera Alta, TO, Italy;* orcid.org/0000-0003-0875-7406; Phone: +393791822311; Email: fabrizio.silveri@gemmate-technologies.com

Authors

Matthew G. Quesne − *School of Chemistry, Cardiff University, Cardiff CF10 3AT, U.K.; UK Catalysis Hub, Research Complex at Harwell, STFC Rutherford Appleton Laboratory, Oxfordshire OX11 0FA, U.K.;* orcid.org/0000-0001-5130-1266

Francesc Viñes − *Departament de Ciència de Materials i Química Física and Institut de Química Teòrica i Computacional (IQTCUB), Universitat de Barcelona, 08028 Barcelona, Spain;* orcid.org/0000-0001-9987-8654

Francesc Illas − *Departament de Ciència de Materials i Química Física and Institut de Química Teòrica i Computacional (IQTCUB), Universitat de Barcelona, 08028 Barcelona, Spain;* orcid.org/0000-0003-2104-6123

C. Richard A. Catlow − *School of Chemistry, Cardiff University, Cardiff CF10 3AT, U.K.; UK Catalysis Hub, Research Complex at Harwell, STFC Rutherford Appleton Laboratory, Oxfordshire OX11 0FA, U.K.; Department of Chemistry, University College London, London WC1 HOAJ, U.K.;* orcid.org/0000-0002-1341-1541

Nora H. de Leeuw − *School of Chemistry, Cardiff University, Cardiff CF10 3AT, U.K.; School of Chemistry, University of Leeds, Leeds LS2 9JT, U.K.;* orcid.org/0000-0002-8271-0545

Complete contact information is available at: https://pubs.acs.org/10.1021/acs.jpcc.1c10180

Author Contributions

The manuscript was written through contributions of all authors. All authors have given approval to the final version of the manuscript. The underlying research was planned through the contribution of all authors and performed primarily by F.S. and M.G.Q. between Cardiff University and Universitat de Barcelona, however, with the supervision and contribution of all authors throughout the duration of the project.

Notes

The authors declare no competing financial interest.

All data created as part of this study are openly available at: http://doi.org/10.17035/d.2022.0162515110.

ACKNOWLEDGMENTS

This work was funded as part of an EPSRC low carbon fuel grant (EP/N009533/1). Computing facilities for this work were provided by ARCCA at Cardiff University, HPC Wales, and through our membership of the U.K.'s Materials Chemistry Consortium (MCC). The U.K. Catalysis Hub is thanked for resources and support provided via membership of the U.K. This work also used the Cirrus UK National Tier-2 HPC Service at EPCC (http://www.cirrus.ac.uk) funded by the University of Edinburgh and EPSRC (EP/P020267/1). Catalysis Hub Consortium is funded by EPSRC (grants EP/R026815/1, EP/K014854/1, and EP/M013219/1). The MCC is funded by EPSRC (EP/F067496). The research of F.V. and F.I. carried out the Universitat de Barcelona has been supported by the Spanish MCIN/AEI/10.13039/501100011033 funded RTI2018-095460-B-I00 and María de Maeztu MDM-2017-0767 grants, including funding from European Union. Further funding was provided by the HPC Europa-3 program, through which F.S. could access the computing facilities of the Barcelona Supercomputing Centre.

ABBREVIATIONS

DFT, density functional theory; PBE, Perdew−Burke−Ernzerhof; PAW, projected-augmented wave; TMC, transition-metal carbide

REFERENCES

(1) Centi, G.; Quadrelli, E. A.; Perathoner, S. Catalysis for CO2 Conversion: A Key Technology for Rapid Introduction of Renewable Energy in the Value Chain of Chemical Industries. *Energy Environ. Sci.* **2013**, *6*, 1711−1731.

(2) Lewis, N. S.; Nocera, D. G. Powering the Planet: Chemical Challenges in Solar Energy Utilization. *Proc. Natl. Acad. Sci. U.S.A.* **2006**, *103*, 15729−15735.

(3) Sulley, G. S.; Gregory, G. L.; Chen, T. T. D.; Peña Carrodeguas, L.; Trott, G.; Santmarti, A.; Lee, K. Y.; Terrill, N. J.; Williams, C. K. Switchable Catalysis Improves the Properties of CO2-Derived Polymers: Poly(Cyclohexene Carbonate- b-ϵ-Decalactone- b-Cyclohexene Carbonate) Adhesives, Elastomers, and Toughened Plastics. *J. Am. Chem. Soc.* **2020**, *142*, 4367−4378.

(4) Quadrelli, E. A.; Centi, G.; Duplan, J. L.; Perathoner, S. Carbon Dioxide Recycling: Emerging Large-Scale Technologies with Industrial Potential. *ChemSusChem* **2011**, *4*, 1194−1215.

(5) Aresta, M.; Dibenedetto, A.; Angelini, A. Catalysis for the Valorization of Exhaust Carbon: From CO2 to Chemicals, Materials, and Fuels. Technological Use of CO2. *Chem. Rev.* **2014**, *114*, 1709−1742.

(6) Ma, J.; Sun, N.; Zhang, X.; Zhao, N.; Xiao, F.; Wei, W.; Sun, Y. A Short Review of Catalysis for CO2 Conversion. *Catal. Today* **2009**, *148*, 221−231.

(7) Quesne, M. G.; Silveri, F.; de Leeuw, N. H.; Catlow, C. R. A. Advances in Sustainable Catalysis: A Computational Perspective. *Front. Chem.* **2019**, *7*, No. 182.

(8) Posada-Pérez, S.; Gutiérrez, R. A.; Zuo, Z.; Ramírez, P. J.; Viñes, F.; Liu, P.; Illas, F.; Rodriguez, J. A. Highly Active Au/δ-MoC and Au/β-Mo2C Catalysts for the Low-Temperature Water Gas Shift Reaction: Effects of the Carbide Metal/Carbon Ratio on the Catalyst Performance. *Catal. Sci. Technol.* **2017**, *7*, 5332−5342.

(9) Kunkel, C.; Viñes, F.; Ramírez, P. J.; Rodriguez, J. A.; Illas, F. Combining Theory and Experiment for Multitechnique Characterization of Activated CO2 on Transition Metal Carbide (001) Surfaces. *J. Phys. Chem. C* **2019**, *123*, 7567−7576.

(10) Porosoff, M. D.; Kattel, S.; Li, W.; Liu, P.; Chen, J. G. Identifying Trends and Descriptors for Selective CO2 Conversion to CO over Transition Metal Carbides. *Chem. Commun.* **2015**, *51*, 6988−6991.

(11) Lim, R. J.; Xie, M.; Sk, M. A.; Lee, J. M.; Fisher, A.; Wang, X.; Lim, K. H. A Review on the Electrochemical Reduction of CO2 in Fuel Cells, Metal Electrodes and Molecular Catalysts. *Catal. Today* **2014**, *233*, 169−180.

(12) Wang, W.; Wang, S.; Ma, X.; Gong, J. Recent Advances in Catalytic Hydrogenation of Carbon Dioxide. *Chem. Soc. Rev.* **2011**, *40*, 3703−3727.

(13) Posada-Pérez, S.; Ramírez, P. J.; Gutiérrez, R. A.; Stacchiola, D. J.; Viñes, F.; Liu, P.; Illas, F.; Rodriguez, J. A. The Conversion of CO2 to Methanol on Orthorhombic β-Mo2C and Cu/β-Mo2C Catalysts: Mechanism for Admetal Induced Change in the Selectivity and Activity. *Catal. Sci. Technol.* **2016**, *6*, 6766−6777.

(14) Quesne, M. G.; Roldan, A.; de Leeuw, N. H.; Catlow, C. R. A. Bulk and Surface Properties of Metal Carbides: Implications for Catalysis. *Phys. Chem. Chem. Phys.* **2018**, *20*, 6905−6916.
(15) Quesne, M. G.; Roldan, A.; De Leeuw, N. H.; Catlow, C. R. A. Carbon Dioxide and Water Co-Adsorption on the Low-Index Surfaces of TiC, VC, ZrC and NbC: A DFT Study. *Phys. Chem. Chem. Phys.* **2019**, *21*, 10750−10760.
(16) Silveri, F.; Quesne, M. G. M. G.; Roldan, A.; De Leeuw, N. H. N. H.; Catlow, C. R. A. R. A. Hydrogen Adsorption on Transition Metal Carbides: A DFT Study. *Phys. Chem. Chem. Phys.* **2019**, *21*, 5335−5343.
(17) Kunkel, C.; Viñes, F.; Illas, F. Transition Metal Carbides as Novel Materials for CO $_2$ Capture, Storage, and Activation. *Energy Environ. Sci.* **2016**, *9*, 141−144.
(18) Kresse, G.; Furthmüller, J. Efficient Iterative Schemes for *Ab Initio* Total-Energy Calculations Using a Plane-Wave Basis Set. *Phys. Rev. B* **1996**, *54*, 11169−11186.
(19) Blöchl, P. E. Projector Augmented-Wave Method. *Phys. Rev. B* **1994**, *50*, 17953−17979.
(20) Perdew, J. P.; Burke, K.; Ernzerhof, M. Generalized Gradient Approximation Made Simple. *Phys. Rev. Lett.* **1996**, *77*, 3865−3868.
(21) Grimme, S.; Antony, J.; Ehrlich, S.; Krieg, H. A Consistent and Accurate Ab Initio Parametrization of Density Functional Dispersion Correction (DFT-D) for the 94 Elements H-Pu. *J. Chem. Phys.* **2010**, *132*, No. 154104.
(22) Blöchl, P. E.; Jepsen, O.; Andersen, O. K. Improved Tetrahedron Method for Brillouin-Zone Integrations. *Phys. Rev. B* **1994**, *49*, 16223.
(23) Piñero, J. J.; Ramírez, P. J.; Bromley, S. T.; Illas, F.; Viñes, F.; Rodriguez, J. A. Diversity of Adsorbed Hydrogen on the TiC(001) Surface at High Coverages. *J. Phys. Chem. C* **2018**, *122*, 28013−28020.
(24) Morales-García, Á.; Fernández-Fernández, A.; Viñes, F.; Illas, F. CO2 Abatement Using Two-Dimensional MXene Carbides. *J. Mater. Chem. A* **2018**, *6*, 3381−3385.
(25) Morales-García, Á.; Mayans-Llorach, M.; Viñes, F.; Illas, F. Thickness Biased Capture of CO2 on Carbide MXenes. *Phys. Chem. Chem. Phys.* **2019**, *21*, 23136−23142.
(26) Rodriguez, J. A.; Liu, P.; Gomes, J.; Nakamura, K.; Viñes, F.; Sousa, C.; Illas, F. Interaction of Oxygen with ZrC(001) and VC(001): Photoemission and First-Principles Studies. *Phys. Rev. B* **2005**, *72*, No. 075427.
(27) Weinberg, W. H. Eley-Rideal Surface Chemistry: Direct Reactivity of Gas Phase Atomic Hydrogen with Adsorbed Species. *Acc. Chem. Res.* **1996**, *29*, 479−487.
(28) Posada-Pérez, S.; Viñes, F.; Ramirez, P. J.; Vidal, A. B.; Rodriguez, J. A.; Illas, F. The Bending Machine: CO2 Activation and Hydrogenation on δ-MoC(001) and β-Mo2C(001) Surfaces. *Phys. Chem. Chem. Phys.* **2014**, *16*, 14912−14921.
(29) Posada-Pérez, S.; Viñes, F.; Ramirez, P. J.; Vidal, A. B.; Rodriguez, J. A.; Illas, F. The Bending Machine: CO_2 Activation and Hydrogenation on δ-MoC(001) and β-Mo_2C(001) Surfaces. *Phys. Chem. Chem. Phys.* **2014**, *16*, 14912−14921.
(30) Wan, W.; Tackett, B. M.; Chen, J. G. Reactions of Water and C1 Molecules on Carbide and Metal-Modified Carbide Surfaces. *Chem. Soc. Rev.* **2017**, *46*, 1807−1823.

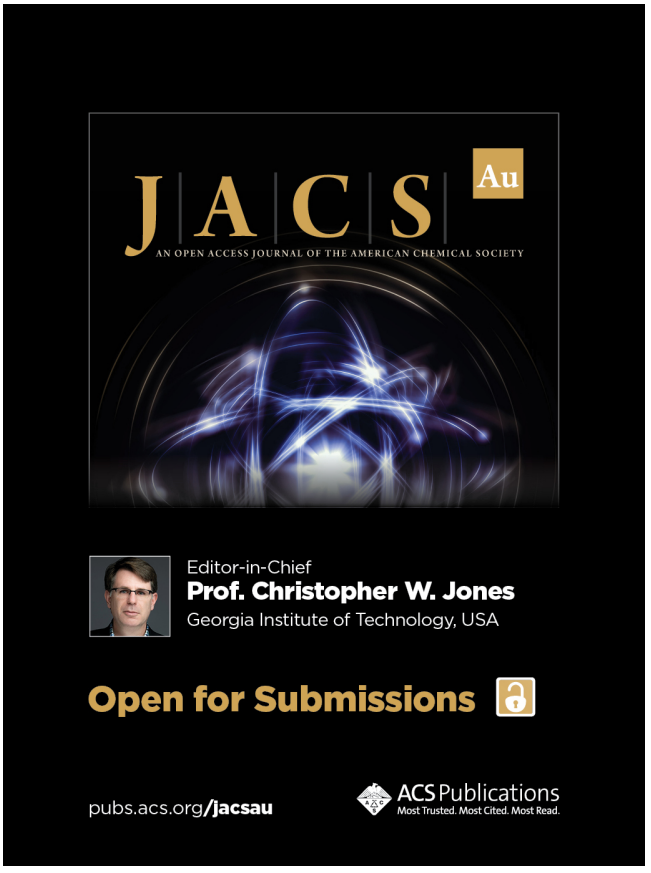

https://doi.org/10.1021/acs.jpcc.1c10180
J. Phys. Chem. C 2022, 126, 5138−5150